# Flexural Strengthening of RC Columns with NSM FRP or Stainless Steel

by Dionysios A. Bournas and Thanasis C. Triantafillou

## Abstract

The paper presents the results of a large-scale experimental program aiming to study the behavior of reinforced concrete (RC) columns under simulated seismic loading, strengthened in flexure (of crucial importance in capacity design) with different types and configurations of near-surface mounted (NSM) reinforcing materials. The role of different parameters is examined, by comparison of the lateral load versus displacement response characteristics (peak force, drift ratios, energy dissipation, stiffness). Those parameters were as follows: carbon or glass fiber-reinforced polymers (FRP) versus stainless steel; configuration and amount of NSM reinforcement; confinement via local jacketing; and type of bonding agent (epoxy resin or mortar). The results demonstrate that NSM FRP and stainless steel reinforcement is a viable solution towards enhancing the flexural resistance of reinforced concrete columns subjected to seismic loads. This is especially the case, when the retrofitting scheme combines epoxy-bonded NSM bars with local confining jackets (provided in this study with textile-reinforced mortars – TRM).

**Keywords:** columns; flexure; near surface mounted reinforcement; seismic retrofitting; strengthening; textile-reinforced mortar (TRM).

## BIOGRAPHICAL SKETCHES

*ACI member* **Dionysios A. Bournas** *is a Postdoctoral researcher in the Department of Civil Engineering at the University of Patras, Greece. He received his diploma in Civil Engineering (2004) and PhD (2008) from the University of Patras. His main research interests include mechanical behavior of concrete and the application of advanced polymer or cement-based composites in combination with concrete, with emphasis on strengthening and seismic retrofitting.*

*ACI member* **Thanasis C. Triantafillou** *is Professor of Civil Engineering and Director of the Structural Materials Laboratory at the University of Patras, Greece. He received his diploma in Civil Engineering from the University of Patras in 1985 and his MSc (1987) and PhD (1989) degrees from the Massachusetts Institute of Technology, where he served as Assistant Professor of Civil and Environmental Engineering from 1990 to 1993. His main research interests include the application of advanced polymer or cement-based composites in combination with concrete, masonry and timber, with emphasis on strengthening and seismic retrofitting. Prof. Triantafillou is the convenor of the fib working party "Externally Bonded Reinforcement" of TG9.3, and member of RILEM technical committees on FRP and textile reinforcement.*

## INTRODUCTION AND BACKGROUND

Earthquakes worldwide have proven the vulnerability of existing reinforced concrete (RC) columns to seismic loading. Poorly detailed columns are the most critical structural elements, which may fail due to shear, compressive crushing of concrete, rebar buckling, bond at lap-splices and flexure. Seismic retrofitting of RC columns is a challenging task that may be addressed successfully today using externally bonded composite materials (Fiber-Reinforced Polymers, FRP) for all the aforementioned failure mechanisms but the last one, that is flexure. FRPs, in the form of jackets with the fibers typically in the columns' circumferential direction, are quite effective in carrying shear and in providing confinement, thus increasing the shear resistance and the deformation capacity of existing RC columns. However, effective strengthening of columns in flexure, often needed for instance to satisfy capacity design requirements (that is the elimination of weakness in strong beam – weak column situations) or when existing rebars have been affected by corrosion, calls for the continuation of longitudinal reinforcement. This reinforcement should extend beyond the end cross sections, where moments are typically maximum. Therefore, placement of externally bonded FRP is not applicable. As a result, flexural strengthening of RC columns is typically achieved today by using RC jackets or some forms of steel jackets, namely steel "cages", also followed by shotcreting. RC jackets or steel cages covered by shotcrete require intensive labor and artful detailing, they increase the dimensions and weight of columns and result in substantial obstruction of occupancy. Moreover, increasing the stiffness of the column will attract a higher force, since forces are distributed according to the relative stiffness of the elements. Therefore, the implementation of a low labor and minimal obstruction flexural strengthening technique for RC columns still remains a challenging task, which is addressed in this study through the use of near-surface mounted (NSM) reinforcement.

NSM reinforcement (also named "grouted reinforcement" or "embedded reinforcement" in the past) involves cutting grooves into the concrete cover and bonding rebars inside the grooves through the use of an appropriate filler (typically epoxy resin or cement-based mortar). The idea of NSM reinforcement was born in Europe for steel rebars in the late 1940s [1], but it was only recently when more durable materials, such as FRPs and high quality

epoxies, become available, that the technique was given substantial attention by the research community and practitioners. Research so far on NSM reinforcement for RC structures has focused on flexural strengthening of beams or slabs with an emphasis on bond aspects [2-18], on shear strengthening of RC beams [19-21] and on flexural strengthening with prestressed NSM FRP bars [22-23]; the most recent research results in these areas are reported in [24].

The only study reported in the international literature on flexural strengthening of columns with NSM reinforcement is that of Barros et al. [25], who tested 1 m (39.37 in.) long cantilever-type RC column specimens under cyclic flexure combined with axial load. In this study the authors reported a substantial increase in the strength of columns with NSM carbon FRP strips compared to control (unstrengthened) specimens. However, no clear conclusions about the specimens' behavior (in terms of deformation capacity and failure modes) under cyclic loading were made, as the tests were terminated before failure was reached, at a tip displacement equal to 20 mm (0.79 in.), corresponding to a drift ratio less than 2%. This paper presents the first systematic study on NSM-based flexural strengthening of RC columns under simulated seismic loading. The investigation addresses column strengthening with durable NSM materials, namely CFRP (carbon FRP) or GFRP (glass FRP), as well as stainless steel rebars. Another innovative aspect in this study is the combination of NSM reinforcement with local jacketing, which comprised the recently developed textile-reinforced mortar (TRM) confining system, described in [26-27]. Details are provided in the following sections.

## RESEARCH SIGNIFICANCE

Columns, the most critical structural elements in RC structures, are often in need of flexural strengthening to satisfy capacity design requirements (relocation of plastic hinges from columns to beams) or when longitudinal rebars have been affected by corrosion. The implementation of a low labor and minimal obstruction flexural strengthening technique for RC columns still remains a challenging task, which is addressed in this study for the first time in a systematic way through the use of near-surface mounted (NSM) reinforcement. Such reinforcement comprises fiber-reinforced polymers (FRP) and also stainless steel, which is

also investigated for the first time here as an NSM reinforcing system for the flexural strengthening of columns. Finally, NSM reinforcements are combined with locally applied jacketing, consisting of the highly-promising recently developed composite material confining systems, namely textile-reinforced mortars (TRM).

## EXPERIMENTAL PROGRAM

### Test specimens and experimental parameters

The experimental program aimed to study the flexural strengthening of old-type non-seismically detailed RC columns with NSM reinforcement and to compare the effectiveness of different flexural strengthening schemes. A total of eleven large-scale RC column specimens with the same geometry were constructed and tested under cyclic uniaxial flexure with constant axial load (Fig. 1a). The specimens were flexure-dominated (that is slender and designed to fail by yielding of the longitudinal rebars) cantilevers, with a height to the point of application of the load (shear span) of 1.6 m (63 in.) (half a typical story height) and a cross section of 250x250 mm (9.84x9.84 in.). To represent old-type columns, specimens were reinforced longitudinally with four 14 mm-diameter (0.55 in.) smooth bars (except for one specimen which had 12 mm [0.47 in.] bars) and 8 mm (0.32 in.) diameter smooth stirrups, closed with 90-degree hooks at both ends, at a spacing of 200 mm (7.87 in.). The geometry of a typical cross section is shown in Fig. 1b.

The specimens were designed such that the effect of a series of parameters on the flexural capacity of RC columns could be investigated. These parameters comprised: type of NSM reinforcement (CFRP strips, GFRP bars, stainless steel rebars); configuration of NSM reinforcement (CFRP strips placed with their large cross section side perpendicular or parallel to the column sides, depending on whether a proper concrete cover is available or not); amount - that is geometrical reinforcing ratio - of NSM or internal reinforcement; type of bonding agent for the NSM reinforcement (epoxy resin versus cement-based mortar); and NSM reinforcement with or without local jacketing at the member ends. A description of the specimens follows next, supported by Fig. 2 and Table 1.

- One specimen was tested without retrofitting, as **Control**.
- **C_Per** was strengthened with two CFRP strips symmetrically placed on each of two opposite sides of the column (those with highest tension/compression). The strips had a

cross section of 16x2 mm (0.63x0.08 in.) and were placed inside 20x10 mm (0.79x0.39 in.) orthogonal grooves with the large cross section side *perpendicular* to the column side (Fig. 2a). This scheme is feasible only if the concrete cover is at least equal to 20 mm (0.79 in.).

- **C_Per_$\rho_{n2}$** was strengthened as C_Per, but with a higher reinforcing ratio for the NSM reinforcement, provided by placing three strips on each column side.
- **C_Per_$\rho_{s2}$** was strengthened as C_Per (that is with two strips per side), but it was initially designed with a lower reinforcing ratio for the internal steel reinforcement. This specimen was reinforced with 12 mm-diameter bars (0.47 in.), whereas all others had 14 mm-diameter bars (0.55 in.).
- **C_Par** was strengthened with two CFRP strips (with dimensions as above) symmetrically placed on each of two opposite sides of the column. The strips were placed inside 20x5 mm (0.79x0.20 in.) grooves but with their large cross section side *parallel* to the column side (Fig. 2b). This scheme is expected to have less favourable bond characteristics compared to C_Per, but it may be easily applied if the concrete cover is small.
- **C_Par_J** had the same NSM reinforcement as C_Par (that is with two strips per side) and an additional confining jacket, which extended from the column base to a height of 600 mm (23.62 in.). The aim of this jacket was mainly to protect the NSM reinforcement against premature failure due to buckling, which may be followed by debonding.
- **G** was strengthened with two 8 mm-diameter (0.31 in.) deformed GFRP bars symmetrically placed on each of two opposite sides of the column. The bars were placed in 20x20 mm (0.79x0.79 in.) square grooves (Fig. 2c).
- **S_R** was strengthened with two 12 mm-diameter (0.47 in.) deformed stainless steel rebars symmetrically placed on each of two opposite sides of the column. The stainless steel rebars were placed in 20x20 mm (0.79x0.79 in.) square grooves (Fig. 2d). As in all specimens above with NSM reinforcement, the bonding agent inside the grooves was epoxy resin.
- **S_M** had the same NSM reinforcement as S_R (that is with two rebars per side), but the bonding agent inside the grooves was a cement-based mortar (Fig. 2e).
- **S_R_J** had the same NSM reinforcement as S_R (that is with two rebars per side) and an additional confining jacket, as used in C_Par_J.

- **S_M_J** had the same NSM reinforcement as S_M and an additional confining jacket, as used in S_R_J.

In summary, except for the control specimen, the specimens' notation is as follows: the first symbol denotes the NSM reinforcing material (C for CFRP strips, G for GFRP bars, S for stainless steel bars); the second symbol in the C series denotes the orientation of the strips (Per for Perpendicular, Par for Parallel); the second symbol in the S series denotes the bonding agent inside the grooves (R for epoxy resin, M for mortar); the third symbol in the C series denotes if there is a different geometrical reinforcing ratio in comparison with all other specimens ($\rho_{n2}$ for the NSM reinforcement, $\rho_{s2}$ for the internal steel reinforcement); and the symbol J denotes the use of jacketing at the column end. It should be noted that the use of mortar versus resin as bonding agent was explored only in the S series and not in the others with FRP as NSM reinforcement because: (a) quite a few studies on the comparison of resin versus mortar as bonding agent of NSM FRP are already available in the literature; and (b) some of these studies [e.g. 7-8] have already proven the inferior bond characteristics of NSM FRP reinforcement bonded with mortar in comparison with resin.

Of crucial importance in the selection of NSM reinforcement was the requirement of equal tensile strength (not area or stiffness) for each of the reinforcing elements (CFRP strips, GFRP bars, stainless steel bars). Given that all these elements are commercial products, this requirement was satisfied by proper combinations of cross section geometries and material strength data. As a result of this choice, the axial stiffness (elastic modulus times cross section area) ratio of CFRP:GFRP:stainless steel was 1:0.7:4.9.

Jacketing at the column ends in specimens C_Par_J, S_R_J and S_M_J was provided by a novel system with confining effectiveness similar to that of conventional FRP wrapping, but with clear advantages over FRP, mainly associated with the use of inorganic mortars instead of epoxy resins [e.g. 26-27]. This system comprised four layers of a textile with equal quantity of carbon fiber rovings in two orthogonal directions, bonded using a cement-based mortar. The term adopted in previous studies for this material is textile-reinforced mortar (TRM).

## Strengthening procedures

For the sake of simplicity, the grooves at the two column sides were pre-formed by mounting plastic rods at proper positions on the molds. It should be noted that this procedure may, in general, affect bond conditions at the bonding agent – concrete interface, as aggregates were not cut, which would have been the case in practice. But this is relevant only when debonding occurs at this interface, which was not the case in the tests reported in this study. More clarifications regarding failure due to debonding are given below. Upon removal of the plastic rods the grooves were cleaned, roughened with a metallic brush and then cleaned by compressed air. Proper anchorage of the NSM reinforcement inside the base blocks was provided by inserting the reinforcement ends in 300 mm (11.81 in.) long 25 mm-diameter (0.98 in.) holes, which were drilled after concrete casting. When their preparation was completed, grooves and holes were filled by injecting the bonding agent using a simple silicone gun (Fig. 3a). The bonding agent was an epoxy adhesive in all cases, except for two of the specimens with stainless steel bars, where a cement-based mortar was used. Afterwards, the NSM reinforcement was placed into position and the excessive bonding material was removed. To ensure better compaction and flowability of the bonding material inside the base block holes, vibration with a 6 mm-diameter (0.24 in.) rod for the epoxy resin and an addendum of 0.2% super-plasticizer per volume in the mortar mix was provided.

For the specimens receiving TRM jacketing a commercial textile with equal quantity of carbon rovings in two orthogonal directions was used (Fig. 3b). Application of the mortar with this textile was made in approximately 2 mm (0.08 in.) thick layers with a smooth metal trowel. After application of the first mortar layer on the dampened concrete surface (dampening was done manually with a water sprayer), the textile was applied and pressed slightly into the mortar, which protruded through all the open areas between fiber rovings. The next mortar layer covered the textile completely and the operation was repeated until four textile layers were applied and covered by the mortar. Of crucial importance in this method, as in the case of epoxy resins, was the application of each mortar layer while the previous one was still in a fresh state.

The four layers TRM jackets extended from the base of each column (a gap of about 10 mm [0.39 in.] was left) to a height of 600 mm (23.62 mm). A photograph of the application

method of textile combined with mortar binder to provide jacketing in one of the specimens used in this study is shown in Fig. 3c.

## Test set up and materials

The columns were fixed into a heavily reinforced 0.5 m-deep (19.68 in.) base block, 1.2x0.5 m (47x19.7 in.) in plan, within which the longitudinal bars were anchored with 50 mm (1.97 in.) radius hooks at the bottom. The 14 mm-diameter (0.55 in.) longitudinal bars had a yield stress of 372 MPa (53.9 ksi), a tensile strength of 433 MPa (62.8 ksi) and an ultimate strain equal to 17% (average values from six specimens); the respective values for the 12 mm-diameter (0.47 in.) bars were 330 MPa (47.8 ksi), 412 MPa (59.8 ksi) and 23%. The corresponding values for the steel used for stirrups were 351 MPa (50.9 ksi), 444 MPa (64.4 ksi) and 19.5%. In order to simulate field conditions, the base blocks and the columns were cast with separate batches of ready-mix concrete (on two consecutive days). Casting of the columns was made with separate batches too, due to the unavailability of a large number of moulds. The compressive strengths on the day of testing the columns, measured on 150x150 mm (5.9x5.9 in.) cubes (average values from three specimens), are presented in Table 1 for all columns. The average compressive strength and standard deviation were equal to 25.8 MPa and 1.07 MPa, respectively, suggesting that the variability in concrete strength would not affect the column test results.

The mechanical properties of CFRP strips and GFRP bars were measured according to the ACI 440.3R-04 guidelines [28]. Mean values for the tensile strength, the elastic modulus and the ultimate strain of CFRP were obtained using a servohydraulic MTS testing machine, whereas those properties for GFRP bars were measured and provided by the bar suppliers (Table 2). The stress-strain behavior of stainless steel, different from that of carbon steel due to the lack of clear yield point, was characterized through tensile testing according to [29]. The conventional yield stress, corresponding to 0.2% plastic strain, the tensile strength, the elastic modulus and the ultimate strain were obtained, as listed in Table 2. From the values of tensile strength given in Table 2 and the cross section areas one can calculate the tensile force for each of the three NSM reinforcements (conventional yield force, in the case of stainless steel) as follows: 69.5 kN (15.62 kip) for the CFRP strips, 74.9 kN (16.84 kip) for the GFRP bars and 75.6 kN (17 kip) for the stainless steel bars.

For the specimens with resin adhesive for bonding of the NSM reinforcement, a commercial structural adhesive (two-part epoxy resin with a mixing ratio 4:1 by weight) was used with a tensile strength of 30 MPa (4351 psi) and an elastic modulus of 4.5 GPa (653 ksi); those properties were measured and provided by the manufacturer. For the specimens with mortar as a binding material for bonding of the NSM reinforcement (stainless steel bars in specimens S_M and S_M_J), a commercial inorganic dry binder was used, consisting of cement and polymers at a ratio of about 8:1 by weight. The water:binder ratio in the mortar was 0.23:1 by weight, resulting in plastic consistency, good workability and high flowability.

Testing of this mortar was carried out on six 40x40x160 mm (1.57x1.57x6.3 in.) hardened mortar prisms, at an age of 28 days, according to EN 1015-11 [30]. The prisms were prepared and cured in the laboratory until testing, in conditions identical to those for the jackets used for confinement (except for the first two days, when the prisms were inside the moulds). The prisms were subjected to three-point bending at a span of 100 mm (3.94 in.) and from the peak load the flexural strength was calculated. Compression testing was carried out on each of the fractured parts using two 40x40 mm (1.57x1.57 in.) bearing steel platens on top and bottom of each specimen. The average flexural and compressive strength values were 6.31 MPa (915 psi) and 17.5 MPa (2538 psi), respectively. The average value for the elastic modulus of the mortar was calculated equal to 8 GPa (1160 ksi).

A commercial textile with equal quantity of carbon fibers in two orthogonal directions was used (Fig. 3b) for the TRM jackets, in combination with the same mortar described above. Each fiber roving was 3 mm (0.12 in.) wide and the clear spacing between rovings was 7 mm (0.28 in.). The weight of carbon fibers in the textile was 348 g/m$^2$ (1.42x10$^{-6}$ lb/in$^2$) and the nominal thickness of each layer (based on the equivalent smeared distribution of fibers in the circumferential direction) was 0.095 mm (0.0037 in.). The mean tensile strength and the elastic modulus of the carbon fiber rovings (as well as of the textile, when the nominal thickness is used) were taken from data sheets equal to 3800 MPa (551 ksi) and 225 GPa (32633 ksi), respectively.

The columns were subjected to lateral cyclic loading which consisted of successive cycles progressively increasing by 5 mm (0.20 in.) of displacement amplitudes in each direction. The loading rate was in the range from 0.2 mm/sec (0.008 in./sec) to 1.1 mm/sec (0.043 in./sec), the higher rate corresponding to a higher displacement amplitude, all in

displacement-control mode. At the same time a constant axial load was applied to the columns, corresponding to 20% of the members' compressive strength, which was calculated by multiplying the gross section area by the strength of concrete corresponding to each column. The lateral load was applied using a horizontally positioned 250 kN (56.2 kip) MTS actuator. The axial load was exerted by a set of four hydraulic cylinders with automated pressure self-adjustment, acting against two vertical rods connected to the strong floor of the testing frame through a hinge (Fig. 1a). As a result of this loading scheme, the variation of axial load during each test was negligible. With this set-up the P-Δ moment at the base section of the column is equal to the axial load times the tip displacement (that is at piston fixing position) of the column, times the ratio of hinge distance from the base (0.25 m [9.84 in.]) and the top (0.25+1.60=1.85 m [72.83 in.]) of the column (that is times 0.25/1.85 = 0.135).

Displacements and axial strains at the plastic hinge region were monitored using six displacement transducers (three on each side, perpendicular to the loading direction) fixed at the cross sections 130 mm (5.12 in.), 260 mm (10.24 in.) and 450 mm (17.72 in.) from the column base, as shown in Fig. 1a and Fig. 4a. The instrumentation also comprised a total of 12 strain gages for each column, which were mounted on one NSM reinforcing element per column side. The six strain gages on each reinforcement were placed as follows (Fig. 4b): (a) four along the anchorage length inside the base block, at distances from the NSM reinforcement's free end equal to 20 mm (0.79 in.), 90 mm (3.54 in.), 160 mm (6.30 in.), and 230 mm (9.05 in.); (b) one at the column end section (base) at a distance equal to 300 mm (11.81 in.) from the reinforcement's free end; and (c) one at a distance of 100 mm (3.94 mm) above the base block. Measurements from the strain gages on each NSM element were used to determine the local bond-slip relationship in the anchorage region as well as the NSM strain (equal to the fracture strain or the strain at debonding) in the section of maximum moment.

## EXPERIMENTAL RESULTS

### General

The response of all columns tested is given in Fig. 5 in the form of load-drift ratio (obtained by dividing the tip displacement with the column's height) loops. The corresponding envelope curves are given in Fig. 6; key results are also presented in Table 3. They include: (a) The peak resistance in the two directions of loading. (b) The drift ratio

corresponding to peak resistance in the two directions of loading. (c) The drift ratio at conventional "failure" of the column, defined as reduction of peak resistance in a cycle below 80% of the maximum recorded resistance in that direction of loading. (d) The degree of strengthening, that is the peak resistance normalized with respect to the peak load sustained by the control specimen in the two directions of loading. (e) The drift ratio at failure normalized with respect to the drift ratio at failure sustained by the control specimen. (f) The observed failure mode.

The performance and failure mode of all tested specimens was controlled by flexure, as expected due to their design characteristics (high value of the shear span ratio L/h = 6.4, relatively low ratio of longitudinal reinforcement). This was an important requirement, as the main objective in this study was to evaluate the effectiveness of NSM reinforcement as a means of flexural strengthening of RC columns. The control specimen attained a peak load of about 33 kN (7.42 kip) and a drift ratio at failure of 6.25%. After yielding of the longitudinal reinforcement, the concrete cover and a part of the core over the lower 200 mm (7.87 in.) of the column disintegrated and bar buckling initiated after the concrete cover spalled off.

With only one exception (column C_Par), all strengthened specimens displayed considerably higher (from about 25% up to about 100%) flexural resistance compared to the control specimen. The response of strengthened columns was not in all cases completely symmetrical in the two directions of loading, due to slight differences of the reinforcements' (internal and NSM) effective depth in each strengthened side. Flexural cracking at the column base started at the early stages of loading and the number of flexural cracks increased and propagated with increasing drift ratios, while inclined cracks propagated in the concrete surface at both sides of the grooves as a result of high pull out forces of the NSM reinforcement for most strengthened specimens. Contrary to the unstrengthened column, the failure of the strengthened specimens was never attributed to buckling of the internal reinforcement, as a significant portion (estimated here based on cross section analysis) of the total force in the compression zone was carried by the NSM reinforcement. However, buckling of the longitudinal internal bars always occurred abruptly after failure of the NSM reinforcement. The pinching observed in many of the hysteresis loops shown in Fig. 5 is attributed to slip of the internal (smooth) bars and to the non-yielding response (in most

specimens) of the NSM reinforcement. The behavior of each strengthened column is described in detail below.

### Columns strengthened with CFRP strips or GFRP bars

The observed failure mode for specimens C_Per, C_Per_$\rho_{n2}$ and C_Per_$\rho_{s2}$ (with the strip large cross section side perpendicular to the strengthened column side) was due to tensile rupture of the CFRP strips at the cross section of maximum moment (column base), as shown in Fig. 7a. Compared with the control specimen, the peak force increased up to about 40% and the attained drift ratio (at peak force) was approximately the same, in the order of 3% (except for specimen C_Per_$\rho_{s2}$ in the push direction). Rupture of the NSM strips resulted in a drop of the applied force, when the mean recorded strains of CFRP at the column base (that is at the location of the major flexural crack) were equal to 0.95%, 0.93% and 0.85% for specimens C_Per, C_Per_$\rho_{n2}$ and C_Per_$\rho_{s2}$, respectively. These values are nearly half the measured ultimate strain in the uniaxial tests, indicating the detrimental effect of cycling on the tensile strength of CFRP. Partial debonding of the strips when subjected to high pull out forces in one direction of loading deprived their lateral restraint in the next loading cycle. As a consequence, the strips became vulnerable to high compressive stresses resulting in local buckling and hence damage, which led to their tensile fracture at strains less than the ultimate uniaxial strain.

Specimen C_Par (with the strip large cross section side parallel to the strengthened column side) displayed rather poor flexural strengthening characteristics: It failed due to early debonding of the CFRP strips at a force marginally higher than the control specimen and a drift ratio of about 2%, with a mean recorded strain of the strips at peak force equal to 0.50%, that is well below their tensile capacity. Debonding of the NSM strips at such a low strain is attributed to their outward spalling due to buckling, as shown in Fig. 7b, rather than to their poor anchoring conditions and the strips' low resistance against pull out. This can be confirmed by examining the results in comparison with specimen C_Par_J, which was identical to C_Par but jacketed at the column end. In this specimen the TRM jacket provided lateral resistance to the strips against buckling, thus increasing the peak force substantially, by 46% and 26% in the push and pull direction, respectively, and the drift ratio at peak force to about 4% and 2.5% in the corresponding directions. The reduced activation of tensile strips in

the pull direction as compared to the push is attributed to their debonding, a fact which is confirmed by the values of mean recorded strains at peak force equal to 1.6% and 0.85% in the push and pull direction, respectively. These values are in agreement with observations of strip tensile rupture in the push direction only.

Specimen G, strengthened with 8 mm-diameter (0.31 in.) GFRP bars, displayed some distinct behavior characteristics: At a drift ratio a little higher than 2% some of GFRP bar ribs experienced shear fracture (Fig. 7c), resulting in slippage between the bars and the epoxy adhesive inside the grooves. The mean recorded strain in the bars when this phenomenon initiated was 0.45%, well below the bars' ultimate strain. In this specimen, failure in both directions was due to buckling of the GFRP bars, at drift ratios in the order of 5%, with a mean recorded strain of GFRP equal to 1.1%; the attained degree of strengthening was about 1.20-1.25.

### Columns strengthened with stainless steel bars

Specimen S_R (with two 12mm-diameter [0.47 in.] stainless steel bars on each retrofitted side) failed when the bars buckled suddenly (Fig. 7d) at a degree of strengthening more than 1.6 and a drift ratio of about 5%, with a buckled length approximately equal to 0.5 m (19.68 in.). Its jacketed counterpart, that is specimen S_R_J, displayed an improved behavior, comprising stable hysteresis loops until large drift ratios, in the order of 8%. This specimen attained the maximum flexural resistance, which was nearly double that of the control specimen. The confinement exerted by the TRM jacket at the base of this specimen restrained buckling of the NSM bars, which fractured in the pull direction, as shown in Fig. 7e, when the tensile strain was approximately equal to 10.1 %. This value is nearly half the measured ultimate strain in the uniaxial tests, indicating again, as in the case of specimens C_Per, C_Per_$\rho_{n2}$ and C_Per_$\rho_{s2}$, the detrimental effect of cycling on the ultimate (monotonic) strain of stainless steel bars.

For specimens S_M and S_M_J with mortar-filled grooves, the relatively low strength of the mortar (in comparison with the epoxy resin) in the base block resulted in gradual pull out of the bars and relative slip between bars and the surrounding mortar in the anchoring region. As a result, the level of force transfer in this region was limited and the effectiveness of the NSM bars was reduced, due to their limited stressing (well below their yield stress). The

damage of the mortar inside the base block increased in a stable manner as the displacement increased up to the peak resistance of the specimens, which was marked at a drift ratio of about 2% for both directions of loading, corresponding to a strengthening degree in the order of 1.25-1.30. Apart from a slight reduction of the lateral load, the post peak response of both specimens was quite stable, displaying a marginal strength degradation to a load level defined by the residual friction between bar and mortar. This pull out resistance due to friction mechanisms resulted in a nearly rigid motion of the stainless steel bars into the anchoring region with practically the same slip along the bonded length, providing to columns S_M and S_M_J a pseudo-ductile behavior.

### Stiffness and energy dissipation

To evaluate further the effectiveness of the various NSM reinforcement configurations, the stiffness and cumulative dissipated energy - computed by summing up the area enclosed within the load versus piston displacement curves - were recorded for each loading cycle and plotted in Fig. 8. Overall, strengthening with the stainless steel NSM rebars resulted in substantial increase in stiffness and dissipated energy, which was maximum in the case of the jacketed column with resin-filled grooves (S_R_J); as conventional failure approached, the stiffness and energy dissipated by this specimen were nearly three times higher than the corresponding values for the unretrofitted column. It should be clarified here that the better performance of NSM stainless steel rebars versus FRP was expected, as the cross sectional area of NSM was selected on the basis of equal strength; hence, steel rebars had an axial stiffness which was about five and seven times higher than that of CFRP and GFRP, respectively.

It should be noted at this point that the increased stiffness of the strengthened columns corresponds, in general, to increased seismic forces. However, this is not of concern and should not lead to the conclusion that the positive effect of strengthening is counterbalanced by the negative effect of stiffening. What is of crucial importance in capacity design, which is typically the reason why flexural strengthening of columns is a demand, is the higher strength of columns versus that of beams. The NSM technique described in this study resulted in a substantial increase of this column-beam flexural strength ratio.

### Effective strain and bond of NSM reinforcement

The maximum tensile strain in the NSM reinforcement is used here to define the "effective" strain, which is summarized in Table 4. This value was calculated as the mean of all NSM strains recorded by strain gages at the column base (cross section of maximum moment) in each loading direction at peak force or at failure for columns S_R and S_R_J. For specimens strengthened with CFRP strips, with their large cross section side perpendicular to the strengthened column side, the effective strain was found to be approximately half of the ultimate uniaxial tensile strain. However, for CFRP strips placed with their large cross section side parallel to the strengthened column side, that is placed inside shallow grooves (C_Par), the effective strain was reduced significantly (27% of the ultimate strain). But in the presence of external confinement through jacketing (column C_Par_J), this strain increased substantially, to about 2/3 of the ultimate uniaxial tensile strain. Similarly, for columns strengthened with stainless steel bars the utilization of the bars' effective tensile strain at failure was substantially higher for the TRM confined specimen S_R_J in comparison with its unconfined counterpart S_R. In general, the increase in the NSM reinforcement's effective strain was favourable to the overall column response, both in terms of strength increase and increase of the deformability at conventional failure.

Although in this study the anchorage length of the NSM reinforcement was not an experimental parameter and a constant value of 300 mm (11.81 in.) was initially selected (to ensure that epoxy-bonded FRPs would not debond inside the base block), the bond behavior of NSM reinforcement along the anchorage length was given some attention for the FRP-retrofitted columns. Figure 9 shows the distribution of axial strain (Fig. 9a) in the FRP reinforcements and the distribution of the bond stress (Fig. 9b) at the FRP-epoxy resin interface, both corresponding to the peak load, for specimens C_Per, C_Per_$\rho_{n2}$, C_Par, C_Par_J and G. Note that bond stresses were calculated at the positions of strain gages by linear interpolation of shear stresses at mid-distances; those shear stresses were derived from adjacent axial strains recorded by the gages. Table 4 also gives the maximum bond stress at the loaded end of the NSM reinforcement (column base) and the average bond stress along the anchorage length for each retrofitted specimen. These measured axial strains and computed bond stresses (maximum and average values) for the specimens tested are consistent with the corresponding increase of the lateral load capacity with respect to the control specimen.

Moreover, such data are quite valuable for modeling the bond of NSM FRP surrounded by concrete, as is the case when NSM reinforcement is anchored in foundation blocks or in beam-column joints. Note that data of this type are not available in the literature, which has focused on bond aspects of NSM reinforcement used to provide flexural strengthening in beam-type members, where bond conditions are less favorable.

## DISCUSSION OF RESULTS

All columns responded as designed and failed by flexural yielding of the internal steel, followed by failure of the NSM reinforcement. In terms of the various factors investigated in this experimental program, an examination of the results (Table 3) in terms of strength (average increase in the push and pull direction), deformation capacity and failure modes, revealed the following information:

*Type of NSM reinforcement* (C_Per versus G versus S_R). Despite the roughly equal (monotonic) uniaxial strength of CFRP, GFRP and stainless steel bars, the latter were more effective, resulting in strength increase equal to 64%. The respective values for FRPs were lower (26% for CFRP and 22% for GFRP), due to failure of the FRP reinforcing elements at strains less than those corresponding to ultimate strains in monotonic loading, as a result of cyclic loading. In terms of deformation capacity, quantified here by the drift ratio at conventional failure, stainless steel and GFRP bars outperformed CFRP strips by approximately 25%, due to the lower deformation capacity of carbon fibers in comparison with the other two materials.

*Geometrical reinforcing ratio of NSM reinforcement* (C_Per versus C_Per_$\rho_{n2}$). Increasing the NSM reinforcing ratio by 50% (three versus two strips in each side) resulted in a nearly proportional increase in strength, that is from 26% in specimen C_Per to 35% in specimen C_Per_ $\rho_{n2}$. Of course, this linearity may not apply in the case of high NSM reinforcing ratios.

*Geometrical reinforcing ratio of internal steel reinforcement* (C_Per versus C_Per_$\rho_{s2}$). Through the use of standard cross-section analysis based analytical modelling (Navier-Bernoulli hypothesis for plane cross sections) and the rectangular stress block approach for concrete in compression (without safety factors), a specimen similar to C_Per_$\rho_{s2}$ but without NSM reinforcement has a predicted strength equal to 26.15 kN. Note that the same analysis

predicted the experimentally obtained strength of the control column with an error of less than 5%, hence this model is considered reliable. By dividing the strength of specimen C_Per_$\rho_{s2}$ (average value in the push and pull direction) with this value, the resulting degree of strengthening is approximately equal to 1.34. Therefore it is verified (and quantified) that the effectiveness of NSM reinforcement increases as the internal steel reinforcing ratio decreases: two NSM strips in each column side increased the strength by 34% for specimen with geometrical ratio of internal steel equal to $\rho_s$=0.724%, whereas the respective increase for the case of $\rho_s$=0.985% was only 26%.

*Configuration of NSM strips* (C_Per versus C_Par). In the absence of local jacketing, NSM strips placed with their large cross section side perpendicular to the column side were far more effective than those with their large cross section side parallel to the column side, due to the more favourable bond conditions. The strength increase in the former case was 26%, but only 4%, that is marginal, in the latter case.

*NSM reinforcement with or without local jacketing* (C_Par versus C_Par_J, S_R versus S_R_J, S_M versus S_M_J). Except for the case of mortar binder inside the grooves, which resulted in NSM debonding at the anchorage, local wrapping of the columns with TRM jackets resulted in substantial improvements of the retrofitted columns' response, by increasing both strength and deformation capacity. Jacketing with TRM improved the bond conditions and restrained buckling of the NSM reinforcement, thereby making the strength increase from 4% to 36% in the case of CFRP and from 64% to 90% in the case of stainless steel. In columns retrofitted with NSM bars placed inside mortar, jacketing offered a marginal increase in strength and a moderate increase in deformation capacity. Of all columns tested, the one retrofitted with the combination of epoxy-bonded stainless steel bars and TRM jacketing displayed the best response characteristics (Fig. 5j), with stable post peak behavior and minimal strength degradation up to large drift ratios. On the basis of the results presented herein, it seems that the combination of NSM flexural strengthening and local jacketing is a viable means for increasing strength without compromising deformation capacity. Note that the latter might be the case in unjacketed columns under low axial loads, as recorded in this study for all columns without jackets (see normalized drift ratios in Table 3). In that respect it should be noted that higher axial loads would result in a lower drift ratio, as also confirmed here by a test of a column identical to the control specimen but with a

normalized axial load equal to 0.3. In that case the drift ratio at failure was 3.75%, that is much lower than 6.25% recorded for the case of normalized axial load equal to 0.2. Hence, the improvements in deformation capacity (in addition to those in strength) are expected higher as axial loads increase.

*Type of bonding agent* (S_R versus S_M, S_R_J versus S_M_J). Epoxy resin was a much more effective bonding agent for NSM stainless steel. For the unjacketed specimens, when mortar was used (S_M) instead of resin (S_R), the increase in strength dropped from 64% to 24%; the corresponding values for jacketed specimens were 90% and 29%. Hence, the use of mortar instead of resin reduced the effectiveness of the strengthening scheme to about 1/3, due to pullout of the NSM stainless steel bars.

## CONCLUSIONS

A systematic study on NSM-based flexural strengthening of RC columns under simulated seismic loading was presented in this paper. The investigation addressed column strengthening with NSM CFRP or GFRP, as well as stainless steel rebars. Another innovative aspect in this study was the combination of NSM reinforcement with local jacketing, which comprised the recently developed textile-reinforced mortar (TRM) confining system. The design of specimens allowed for an investigation of several variables, details of which are given above. The main conclusions are summarized in a rather qualitative manner as follows:

- NSM FRP or stainless steel reinforcement is a viable solution towards enhancing the flexural resistance of reinforced concrete columns subjected to seismic loads. With proper design, which should combine compulsory NSM reinforcement with local jacketing at column ends, it seems that column strength enhancement does not develop at the expense of low deformation capacity.
- NSM CFRP strips perform quite effectively even when a very low concrete cover is available, that is with their large cross section side parallel to the column side, provided that local jacketing is constructed at the column ends.
- As expected, NSM CFRP strips and GFRP bars with equal axial strength are equally effective in terms of strength; GFRP was proven to be slightly superior in terms of deformation capacity.

- All types of NSM reinforcing elements (bonded with epoxy resin) reached large axial strains; however, due to the effect of load cycling, those strains were well below ultimate values recorded during monotonic uniaxial testing. Hence, a comparison of the various NSM materials on the basis of equal uniaxial tension bar strength is in favor of stainless steel, which exhausted its load capacity due to yielding. Therefore, this comparison would make more sense if done on the basis of "effective" strengths mobilized by the different NSM reinforcing elements under cyclic loading.
- Local confinement with TRM jackets is quite effective in controlling buckling of the NSM reinforcement, thus enabling this reinforcement to reach higher strains at failure.
- Epoxy-based bonding agents inside the grooves outperform their cement-based mortar counterparts.

The authors' view is that column strengthening with NSM reinforcement is an area with great potential, hence future research should be directed towards providing a better understanding of parameters including the level of axial load, initial column damage, different shear spans, different loading histories, other cross sections, and other types of FRP reinforcing elements.

## ACKNOWLEDGEMENTS

The authors wish to thank Lecturer C. Papanicolaou, Assoc. Prof. S. Bousias and the students K. Zygouris, F. Stavropoulos and I. Papantoniou for their assistance in the experimental program. GFRP bars were donated by Schöck Bauteile GmbH. The work reported in this paper was funded by the Greek General Secretariat for Research and Technology through the project ARISTION, within the framework of the program "Built Environment and Management of Seismic Risk".

## NOTATION

$A_g$ = gross section area

$E$ = elastic modulus

$f_c$ = compressive strength of concrete

$f_u$ = tensile strength

$f_y$ = yield stress of internal longitudinal reinforcement

$h$ = cross section height

$K$ = stiffness

$L$ = length

$x$ = distance from free end of NSM reinforcement

$\varepsilon_{eff}$ = effective strain

$\varepsilon_u$ = ultimate strain

$\rho_n$ = geometrical ratio of NSM reinforcement

$\rho_s$ = geometrical ratio of internal steel

## REFERENCES

1. Asplund, S. O., "Strengthening Bridge Slabs with Grouted Reinforcement", *ACI Structural Journal*, V. 20, No. 4, 1949, pp. 397-406.

2. Blaschko, M., and Zilch, K., "Rehabilitation of Concrete Structures with Strips Glued into Slits", *Proceedings of the 12th International Conference on Composite Materials*, Paris, 1999 (CD-ROM).

3. Carolin, A., Nordin, H., and Täljsten, B., "Concrete Beams Strengthened with Near Surface Mounted Reinforcement of CFRP", *Proceedings of the International Conference on FRP Composites in Civil Engineering, Research Centre for Advanced Technology in Structural Engineering, Dept. of Civil and Structural Engineering, The Hong Kong Polytechnic Univ.,* Hong Kong, V. II, 2001, pp. 1059-1066.

4. De Lorenzis, L., and Nanni, A., "Bond between Near-Surface Mounted Fiber-Reinforced Polymer Rods and Concrete in Structural Strengthening", *ACI Structural Journal*, V. 99, No. 2, 2002, pp. 123-132.

5. Hassan, T., and Rizkalla, S., "Investigation of Bond in Concrete Structures Strengthened with Near Surface Mounted Carbon Fiber Reinforced Polymer Strips", *ASCE Journal of Composites for Construction*, V. 7, No. 3, 2003, pp. 248-257.

6. Harmon, T., Kim, Y. J., Kardos, J. Johnson, T., and Stark, A., "Bond of Surface-Mounted Fiber-Reinforced Polymer Reinforcement for Concrete Stuctures", *ACI Structural Journal*, V. 100, No. 5, 2003, pp. 557-564.

7. Täljsten, B., Carolin, A., and Nordin, H., "Concrete Structures Strengthened with Near Surface Mounted Reinforcement of CFRP", *Advances in Structural Engineering,* V. 6, No. 3, 2003, pp. 201-213.

8. De Lorenzis, L., Lundgren, K., and Rizzo, A., "Anchorage Length of Near-Surface Mounted Fiber-Reinforced Polymer Bars for Concrete Strengthening – Experimental Investigation and Numerical Modeling", *ACI Structural Journal*, V. 101, No. 2, 2004, pp. 269-278.

9. De Lorenzis, L., "Anchorage Length of Near-Surface Mounted Fiber-Reinforced Polymer Rods for Concrete Strengthening – Analytical Modeling", *ACI Structural Journal*, V. 101, No. 3, 2004, pp. 375-386.

10. El-Hacha, R., and Rizkalla, S., "Near-Surface-Mounted Fiber-Reinforced Polymer Reinforcements for Flexural Strengthening of Concrete Structures", *ACI Structural Journal*, V. 101, No. 5, 2004, pp. 717-726.

11. Hassan, T., and Rizkalla, S., "Bond Mechanism of Near-Surface-Mounted Fiber-Reinforced Polymer Bars for Flexural Strengthening of Concrete Structures", *ACI Structural Journal*, V. 101, No. 6, 2004, pp. 830-839.

12. Sena-Cruz, J. M., and Barros, J. A. O., "Modeling of Bond between Near-Surface Mounted CFRP Laminate Strips and Concrete", *ASCE Journal of Composites for Construction*, V. 8, No. 6, 2004, pp. 519-527.

13. Sena-Cruz, J. M., and Barros, J. A. O., "Bond between Near-Surface Mounted Carbon-Fiber-Reinforced Polymer Laminate Strips and Concrete", *Computers and Structures*, V. 82, No. 17-19, 2004, pp. 1513-1521.

14. Novidis, D., and Pantazopoulou, S. J., "Pullout Tests of NSM-FRP Bars in Concrete", *Proceedings of the 3rd International Conference on Composites in Construction,* Lyon, France, 2005 (CD-ROM).

15. Kotynia, R., "Strain Efficiency of Near-Surface Mounted CFRP-Strengthened Reinforced Concrete Beams", *Proceedings of the 3rd International Conference on Composites in Construction,* Lyon, France, 2005 (CD-ROM).

16. Liu, I. S. T., Oehlers, D. J., and Seracino, R., "Tests on the Ductility of Reinforced Concrete Beams Retrofitted with FRP and Steel Near-Surface Mounted Plates", *ASCE Journal of Composites for Construction*, V. 10, No. 2, 2006, pp. 106-114.

17. Teng, J. G., De Lorenzis, L., Wang, B., Li, R., Wong, T. N., and Lam, L., "Debonding Failures of RC Beams Strengthened with Near Surface Mounted CFRP Strips", *ASCE Journal of Composites for Construction*, V. 10, No. 2, 2006, pp. 92-105.

18. Borchert, K., and Zilch, K., "A General Bond Stress – Slip Relationship for NSM FRP Strips", *Proceedings of the FRPRCS-8 International Symposium,* University of Patras, Greece, 2007, paper ID 8-1.

19. De Lorenzis, L., and Nanni, A., "Shear Strengthening of Reinforced Concrete Beams with NSM Fiber-Reinforced Polymer Rods", *ACI Structural Journal*, V. 98, No. 1, 2001, pp. 60-68.

20. De Lorenzis, L., and Rizzo, A., "Behavior and Capacity of RC Beams Strengthened in Shear with NSM FRP Reinforcement", *Proceedings of the 2nd International fib Congress,* Naples, Italy, 2006 (CD-ROM, paper ID 10-9).

21. Dias, S. J. E., and Barros, J. A. O., "NSM CFRP Laminates for the Shear Strengthening of T Section RC Beams", *Proceedings of the 2nd International fib Congress,* Naples, Italy, 2006 (CD-ROM, paper ID 10-58).

22. Nordin, H., and Täljsten, B., "Concrete Beams Strengthened with Prestressed Near Surface Mounted CFRP", *ASCE Journal of Composites for Construction*, V. 10, No. 1, 2006, pp. 60-68.

23. Casadei, P., Galati, N., Boschetto, G., Tan, K. Y., and Nanni, A., "Strengthening of Impacted Prestressed Concrete Bridge I-Girder using Prestressed Near Surface Mounted C-FRP Bars", *Proceedings of the 2nd International fib Congress,* Naples, Italy, 2006 (CD-ROM, paper ID 10-76).

24. Triantafillou, T. C., editor, *Fiber-Reinforced Polymer Reinforcement for Concrete Structures - Proceedings of the 8th International Symposium on Fiber Reinforced Polymer Reinforcement for Concrete Structures*, University of Patras, Greece, 2007 (www.frprcs8.upatras.gr).

25. Barros, J. A. O., Ferreira, D. R. S. M., Fortes, A. S., and Dias, S. J. E., "Assessing the Effectiveness of Embedding CFRP Laminates in the Near Surface for Structural Strengthening", *Construction and Building Materials*, V. 20, No. 7 , 2006, pp. 478-491.

26. Triantafillou, T. C., Papanicolaou, C. G., Zissimopoulos, P., and Laourdekis, T., "Concrete Confinement with Textile-Reinforced Mortar Jackets", *ACI Structural Journal*, V. 103, No. 1, 2006, pp. 28-37.

27. Bournas, D. A., Lontou, P. V., Papanicolaou, C. G. and Triantafillou, T. C., "Textile-Reinforced Mortar (TRM) versus FRP Confinement in Reinforced Concrete Columns", *ACI Structural Journal*, V. 104, No. 6, 2007, pp. 740-748.

28. ACI 440.3R-04, "Guide Test Methods for Fiber-Reinforced Polymers (FRPs) for Reinforcing or Strengthening Concrete Structures", American Concrete Institute, October 2004.

29. EN ISO 15630-1, *Steel for the Reinforcement and Prestressing of Concrete – Test Methods – Part 1: Reinforcing Bars and Wires*, International Standardisation Organisation, 2002.

30. EN 1015-11, *Methods of Test for Mortar for Masonry – Part 11: Determination of Flexural and Compressive Strength of Hardened Mortar*, European Committee for Standardization, Brussels, Belgium, 1993.

## LIST OF FIGURES

Fig. 1 (a) Schematic of test setup. (b) Cross section of columns. [Dimensions in mm, those in ( ) in inches].

Fig. 2 Detail of NSM reinforcement configuration in columns: (a) C_Per, C_Per_$\rho_{n2}$, C_Per_$\rho_{s2}$; (b) C_Par and C_Par_J; (c) G; (d) S_R and S_R_J; and (e) S_M and S_M_J. [Dimensions in mm, those in ( ) in inches].

Fig. 3 (a) Filling of holes in the anchorage region with epoxy resin or cement-mortar. (b) Photograph of textile used in this study. (c) Application of TRM jacket.

Fig. 4 (a) Position of displacement transducers. (b) Position of strain gages. [Dimensions in mm, those in ( ) in inches].

Fig. 5 Load versus drift ratio curves for tested specimens.

Fig. 6 Load versus drift ratio envelope curves.

Fig. 7 Typical photographs of various failure modes: (a) Tensile fracture of NSM CFRP in columns C_Per, C_Per_$\rho_{n2}$, C_Per_$\rho_{s2}$; (b) Debonding and buckling of NSM CFRP in column C_Par; (c) Shear fracture of GFRP ribs in column G; (d) Buckling of NSM stainless steel bars in column S_R; and (e) tensile fracture of NSM stainless steel bars in column S_R_J.

Fig. 8 (a) Cumulative dissipated energy during test. (b) Stiffness versus drift ratio.

Fig. 9 (a) FRP axial strains and (b) bond stresses in Specimen C_Per, C_Per_$\rho_{f2}$, C_Par, C_Par_J and G.

**TABLE 1 – Experimental parameters**

| Specimen notation | Compressive strength $f_c$, MPa (ksi) | Type of NSM reinforcement | Geometrical ratio of internal reinforcement $\rho_s$, % | Geometrical ratio of NSM reinforcement $\rho_n$, % | Binder | Placement of CFRP strips into grooves | Column end jacket (TRM) |
|---|---|---|---|---|---|---|---|
| Control | 25.6 (3712) | -- | 0.985 | -- | -- | -- | No |
| C_Per | 27.2 (3945) | CFRP strips | 0.985 | 0.205 | Resin | Perpendicular | No |
| C_Per_$\rho_{n2}$ | 27.3 (3959) | CFRP strips | 0.985 | 0.307 | Resin | Perpendicular | No |
| C_Per_$\rho_{s2}$ | 26.8 (3894) | CFRP strips | 0.724 | 0.205 | Resin | Perpendicular | No |
| C_Par | 26.2 (3800) | CFRP strips | 0.985 | 0.205 | Resin | Parallel | No |
| C_Par_J | 25.0 (3626) | CFRP strips | 0.985 | 0.205 | Resin | Parallel | Yes |
| G | 25.1 (3640) | GFRP bars | 0.985 | 0.322 | Resin | -- | No |
| S_R | 26.7 (3873) | Stainless steel bars | 0.985 | 0.724 | Resin | -- | No |
| S_M | 24.4 (3539) | Stainless steel bars | 0.985 | 0.724 | Mortar | -- | No |
| S_R_J | 25.8 (3742) | Stainless steel bars | 0.985 | 0.724 | Resin | -- | Yes |
| S_M_J | 24.3 (3524) | Stainless steel bars | 0.985 | 0.724 | Mortar | -- | Yes |

**TABLE 2 – Mechanical properties of NSM reinforcement**

| Type of NSM reinforcement | Elastic modulus E, GPa (ksi) | Yield stress $f_y$, MPa (ksi) | Tensile strength $f_u$, MPa (ksi) | Ultimate strain $\varepsilon_u$, % |
|---|---|---|---|---|
| CFRP strips | 144.9 (21016) | -- | 2173 (315) | 1.83 |
| GFRP bars | 65.2 (9456) | -- | 1491 (216) | 3.18 |
| Stainless steel bars | 200 (29008) | 668.94 (97) | 761 (110) | 19.15 |

## TABLE 3 – Summary of test results

| Specimen notation | Peak force, kN (kip) | | Drift ratio at peak force, % | | Drift ratio at "failure", % | | Degree of strengthening $\left(\frac{P_{max,Specimen}}{P_{max,Control}}\right)$ | | Normalized drift ratio $\left(\frac{Specimen}{Control}\right)$ | | Failure Mode |
|---|---|---|---|---|---|---|---|---|---|---|---|
| | Push | Pull | Push | Pull | Push | Pull | Push | Pull | Push | Pull | |
| Control | 33.08 (7.44) | -33.69 (-7.57) | 2.81 | -4.68 | 6.25 | -6.25 | 1.00 | 1.00 | 1.00 | 1.00 | B of longitudinal bars |
| C_Per | 41.50 (9.33) | -42.72 (-9.60) | 2.81 | -3.44 | 3.75 | -4.68 | 1.25 | 1.27 | 0.60 | 0.75 | F of NSM strips |
| C_Per_$\rho_{n2}$ | 46.26 (10.40) | -43.82 (-9.85) | 2.81 | -2.81 | 4.06 | -3.13 | 1.40 | 1.30 | 0.65 | 0.50 | F of NSM strips |
| C_Per_$\rho_{s2}$ | 36.25 (8.15) | -33.94 (-7.63) | 1.87 | -2.81 | 3.75 | -3.75 | --[1] | --[1] | --[1] | --[1] | F of NSM strips |
| C_Par | 34.55 (7.77) | -35.03 (-7.87) | 1.87 | -1.87 | 3.44 | -4.38 | 1.04 | 1.04 | 0.55 | 0.70 | D of NSM strips |
| C_Par_J | 48.20 (10.84) | -42.45 (-9.54) | 4.38 | -2.5 | 6.87 | -5.93 | 1.46 | 1.26 | 1.10 | 0.95 | F/D of NSM strips |
| G | 39.58 (8.90) | -42.03 (-9.45) | 3.75 | -3.75 | 5.31 | -5.31 | 1.20 | 1.25 | 0.85 | 0.85 | B of GFRP bars |
| S_R | 52.73 (11.85) | -56.52 (-12.71) | 4.38 | -3.75 | 5.31 | -5.31 | 1.59 | 1.68 | 0.85 | 0.85 | B of stainless steel bars |
| S_R_J | 59.24 (13.32) | -67.70 (-15.22) | 5.31 | -6.25 | >7.81[2] | 7.81 | 1.79 | 2.01 | >1.25[2] | 1.25 | F of stainless steel bar |
| S_M | 41.31 (9.27) | -41.45 (-9.32) | 2.18 | -2.18 | 5 | -5 | 1.25 | 1.23 | 0.80 | 0.80 | PO in the anchorage |
| S_M_J | 42.03 (9.45) | -44.32 (-9.96) | 2.18 | -2.18 | 7.81 | >7.81[2] | 1.27 | 1.31 | 1.25 | >1.25[2] | PO in the anchorage |

B: indicates buckling; F: indicates fracture; D: indicates debonding; PO: indicates pull out failure.

[1] Not applicable, as the control and retrofitted specimens had different internal steel reinforcing ratios.

[2] Maximum stroke of piston was reached.

## TABLE 4 – Bond stresses and effective strain of NSM reinforcement

| Specimen notation | Maximum bond stress at loaded end, MPa (psi) | Average bond stress along the bond length, MPa (psi) | Maximum strain of NSM reinforcement (effective strain $\varepsilon_{eff}$, %) | $\varepsilon_{eff}/\varepsilon_u$ |
|---|---|---|---|---|
| C_Per | 8.25 (1197) | 4.07 (590) | 0.95 | 0.52 |
| C_Per_$\rho_{n2}$ | 9.76 (1416) | 3.91 (567) | 0.93 | 0.51 |
| C_Per_$\rho_{s2}$ | Unreliable recordings | Unreliable recordings | 0.85 | 0.46 |
| C_Par | 4.57 (663) | 2.01 (291) | 0.50 | 0.27 |
| C_Par_J | 11.75 (1704) | 5.93 (860) | 1.23 | 0.67 |
| G | 11.56 (1677) | 5.61 (814) | 1.10 | 0.35 |
| S_R | Not available | Not available | 1.68[1] | 0.09 |
| S_R_J | 16.94 (2457) | 10.57 (1533) | 10.12[1] | 0.53 |
| S_M | 7.59 (1101) | 6.02 (873) | 0.18 | 0.009 |
| S_M_J | 5.77 (837) | 4.21 (611) | 0.26 | 0.014 |

[1] Estimated values from measurements obtained by displacement transducers.

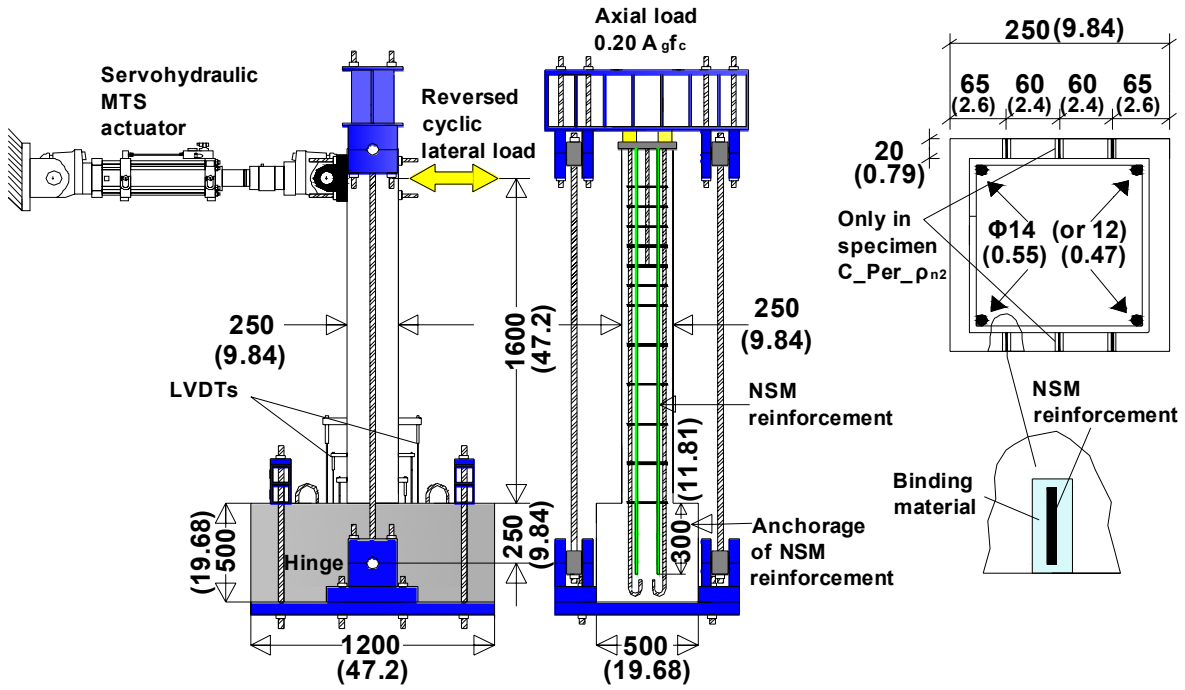
Axial load
0.20 A gfc
Servohydraulic
MTS
actuator
Reversed
cyclic
lateral load
250
(9.84)
1600
(47.2)
250
(9.84)
LVDTs
NSM
reinforcement
(19.68)
500
Hinge
250
(9.84)
300
(11.81)
Anchorage
of NSM
reinforcement
1200
(47.2)
500
(19.68)
250 (9.84)
65 60 60 65
(2.6) (2.4) (2.4) (2.6)
20
(0.79)
Only in
specimen
C_Per_ρn2
Φ14 (or 12)
(0.55) (0.47)
NSM
reinforcement
Binding
material

(a) (b)

Fig. 1

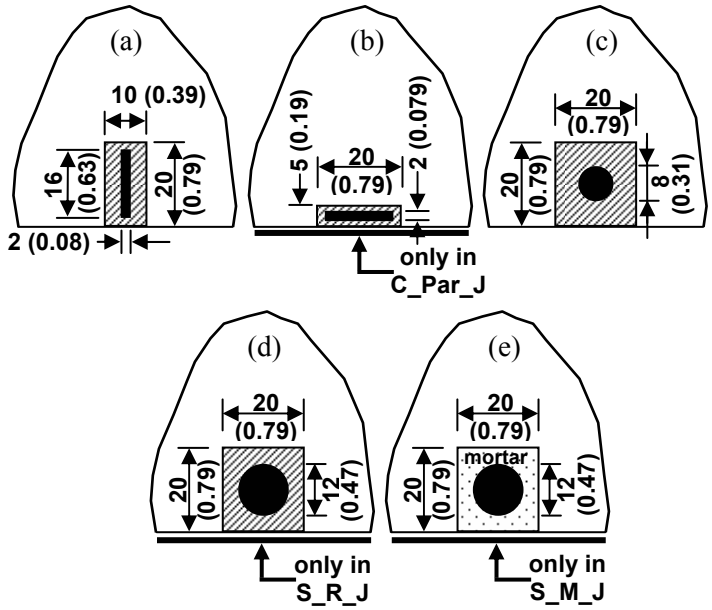
(a)
10 (0.39)
16
(0.63)
20
(0.79)
2 (0.08)
(b)
5 (0.19)
20
(0.79)
2 (0.079)
only in
C_Par_J
(c)
20
(0.79)
20
(0.79)
8
(0.31)
(d)
20
(0.79)
20
(0.79)
12
(0.47)
only in
S_R_J
(e)
20
(0.79)
mortar
20
(0.79)
12
(0.47)
only in
S_M_J

Fig. 2

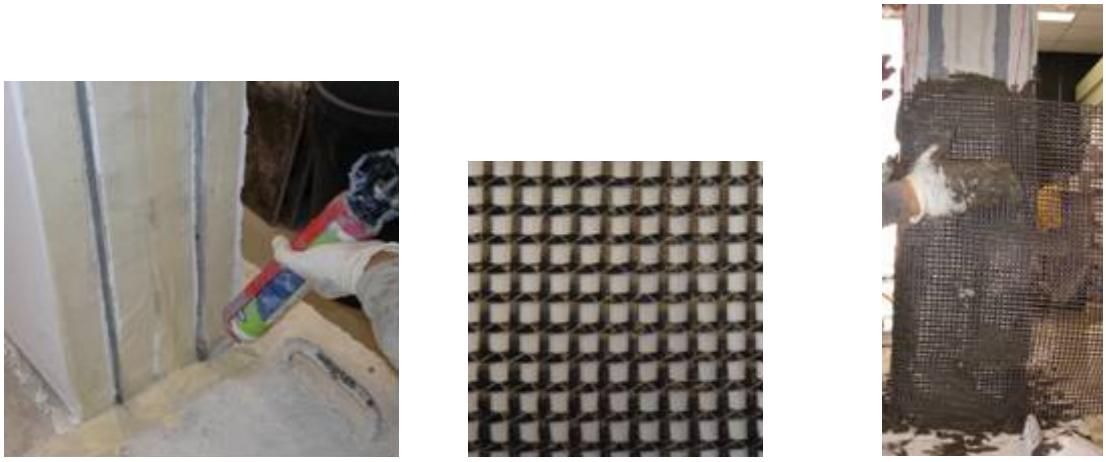

(a) (b) (c)

Fig. 3

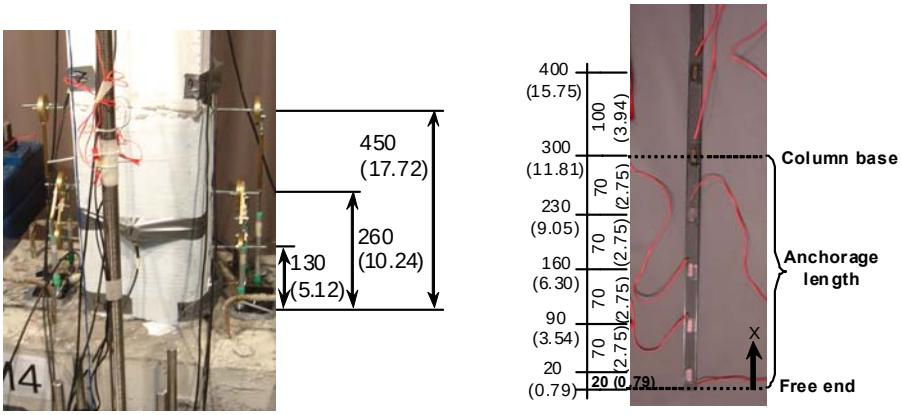


(a) (b)

Fig. 4

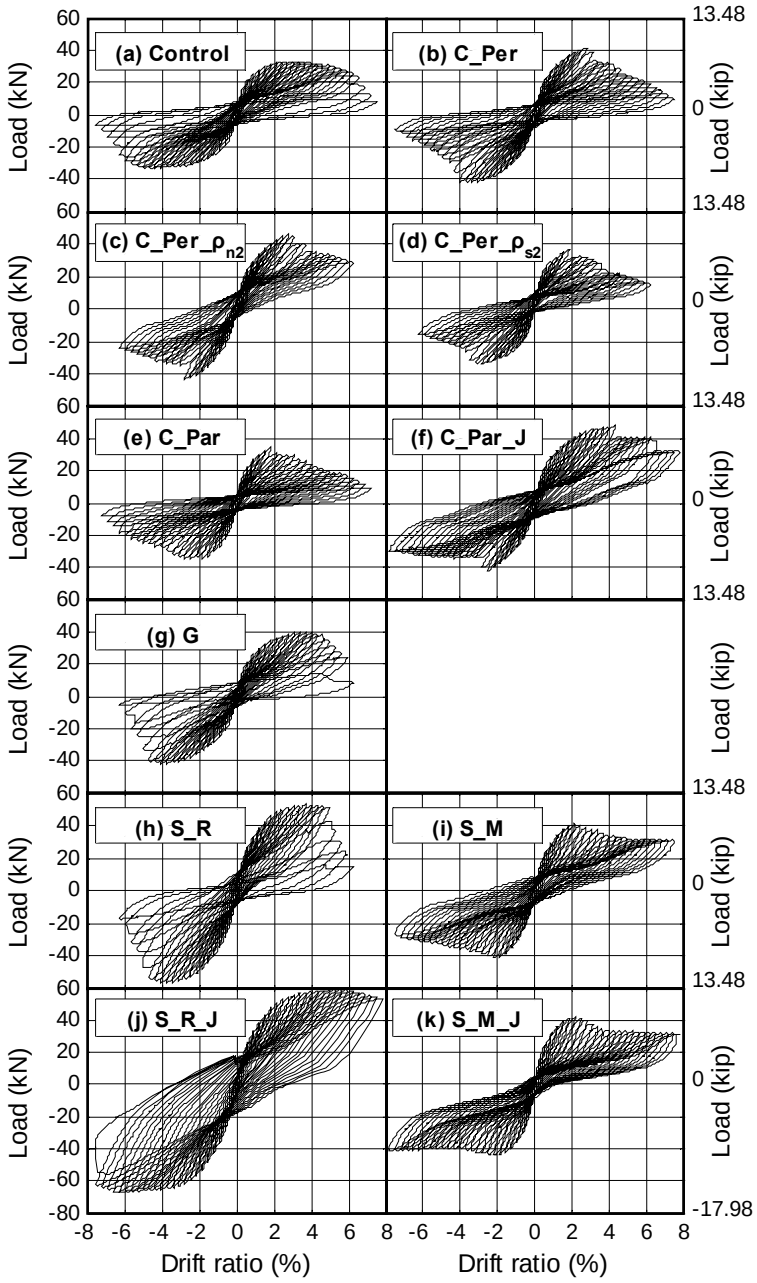
(a) Control
(b) C_Per
(c) C_Per_ρn2
(d) C_Per_ρs2
(e) C_Par
(f) C_Par_J
(g) G
(h) S_R
(i) S_M
(j) S_R_J
(k) S_M_J
Load (kN)
Load (kip)
Drift ratio (%)
60
40
20
0
-20
-40
-60
-80
13.48
0
-17.98
-8 -6 -4 -2 0 2 4 6 8

Fig. 5

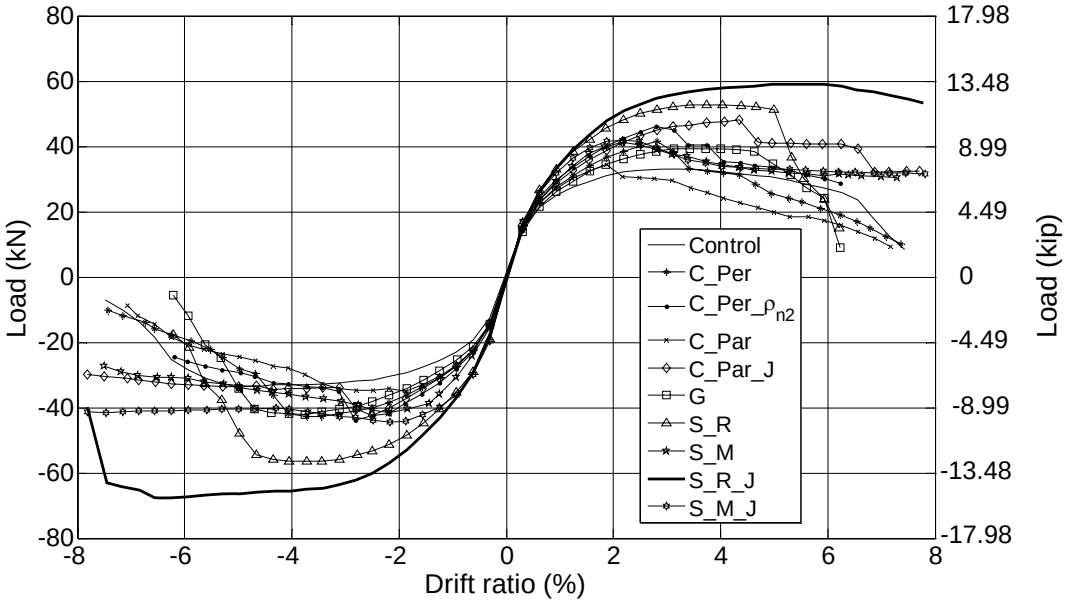


Fig. 6

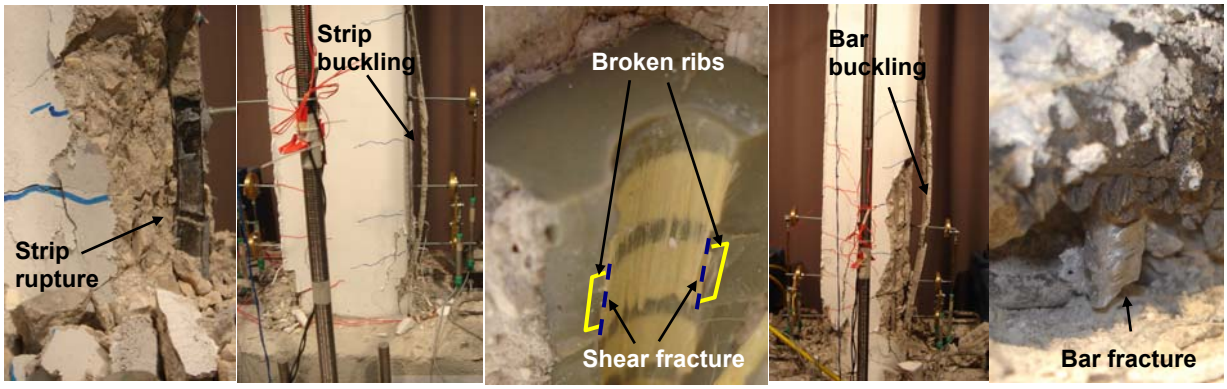


(a) (b) (c) (d) (e)

Fig. 7

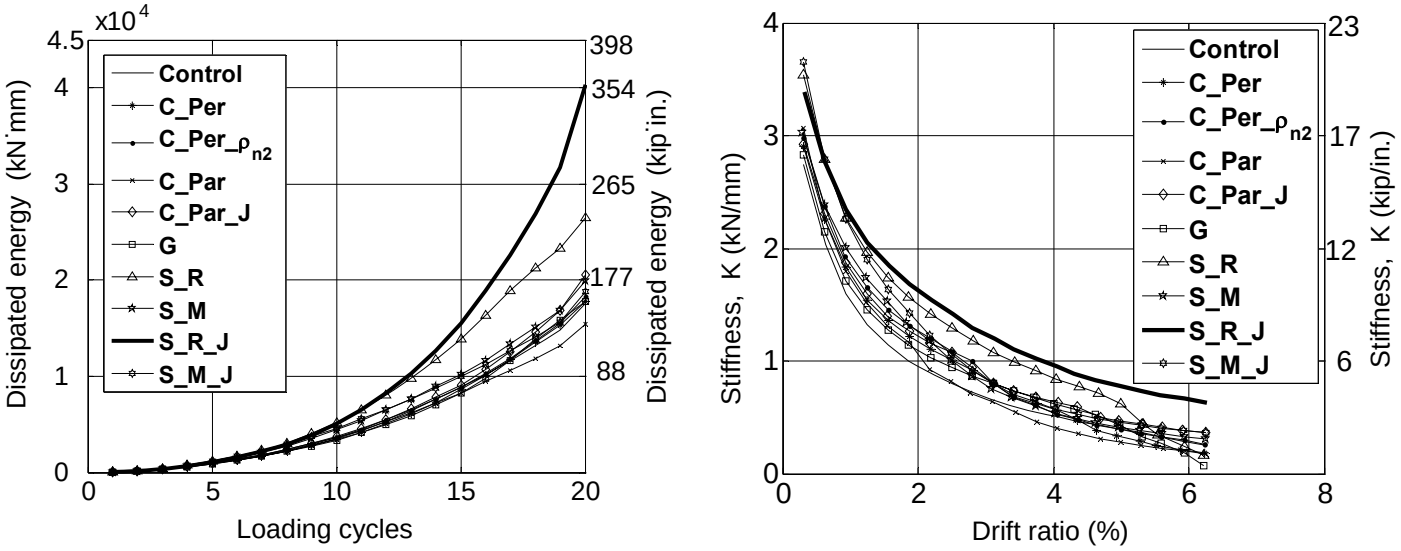


(a) (b)

Fig. 8

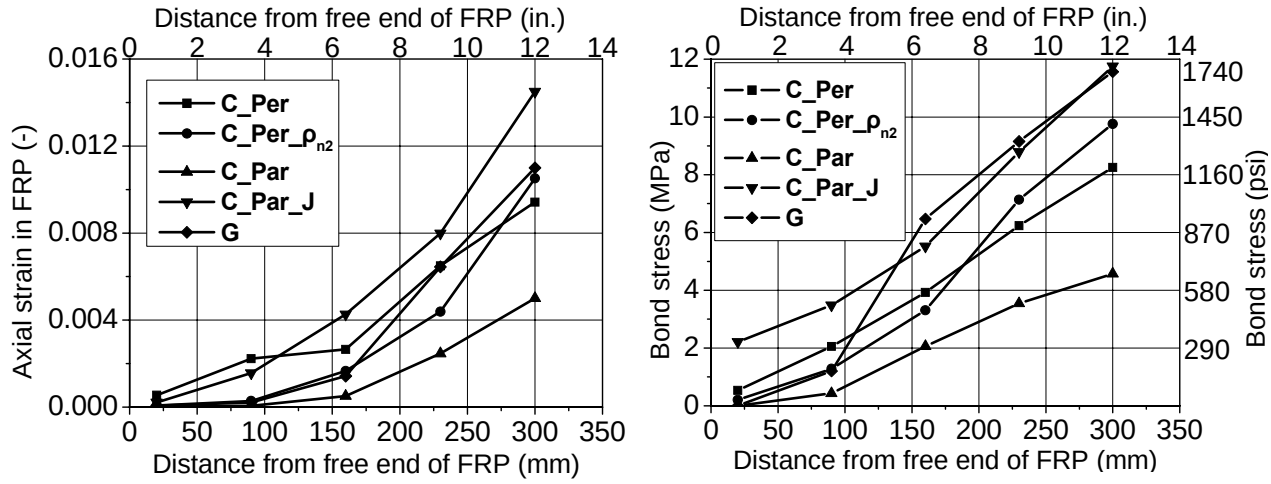


(a) (b)

Fig. 9